



Cite this: DOI: 10.1039/c7gc00269f

Received 22nd January 2017,

Accepted 24th March 2017

DOI: 10.1039/c7gc00269f

rsc.li/greenchem

Direct one-pot conversion of monosaccharides into high-yield 2,5-dimethylfuran over a multifunctional Pd/Zr-based metal–organic framework@ sulfonated graphene oxide catalyst†

Rizki Insyani,^a Deepak Verma,^{a,c} Seung Min Kim ^b and Jaehoon Kim ^{*a,c}

A one-pot conversion of monosaccharides (fructose and glucose) into high-yield 2,5-dimethylfuran (2,5-DMF) is demonstrated over a multifunctional catalyst obtained by loading Pd on a Zr-based metal–organic framework (UiO-66) that is deposited on sulfonated graphene oxide (Pd/UiO-66@SGO). The Brønsted acidity associated with UiO-66@SGO activates the fructose dehydration to form 5-hydroxymethylfurfural (5-HMF), while the Pd nanoparticles further convert 5-HMF to 2,5-DMF by hydrogenolysis and hydrogenation. The results show that under the optimized reaction conditions of 160 °C and 1 MPa H₂ in tetrahydrofuran for 3 h, the yield of 2,5-DMF is as high as 70.5 mol%. This value is higher than the previously reported values, and the direct conversion of fructose can be achieved without additional purification of 5-HMF from the reaction mixture. In addition, for the first time, glucose is converted to 2,5-DMF with a high yield of 45.3 mol%. A recyclability test suggests that the 4.8 wt% Pd loaded on the UiO-66@SGO catalyst can be re-used up to five times.

boiling point (93 °C), and calorific value (34 MJ kg⁻¹) together with a very low water solubility (2.3 g L⁻¹).^{1,4} In addition, 2,5-DMF can be used as a building-block for producing highly valuable aromatic chemical compounds (*e.g.*, *p*-xylene) *via* Diels–Alder reactions.^{5,6}

Despite the many advantages of 2,5-DMF as a renewable fuel and chemical, the direct one-pot conversion of monosaccharides (glucose and fructose) into high-yield 2,5-DMF is still a great challenge. So far, the main approach for the production of 2,5-DMF from monosaccharides involved two-steps: (1) the dehydration of monosaccharides to 5-hydroxymethylfurfural (5-HMF) in the presence of a Lewis or Brønsted acid, (2) the hydrogenolysis of 5-HMF to 2,5-DMF over a metal supported catalysts, as listed in Table S1.†^{1,7–10} In the case of the production of 5-HMF from fructose, various types of homogenous and heterogeneous acid catalysts (*e.g.*, HCl + CrCl₃,¹¹ HCOOH + H₂SO₄,³ SO₄²⁻/ZrO₂–TiO₂,¹² C–SO₃H,¹³ and Amberlyst-15 (ref. 7)) have been tested. For example, Choudhary *et al.* reported that the use of HCl as a Brønsted acid for the dehydration of fructose in the presence of CrCl₃ in a biphasic solvent system composed of THF and water could result in 59 mol% 5-HMF yield.¹¹ Recently, a significantly high 5-HMF yield of 98 mol% was achieved using a modified Zr-based metal–organic framework (NUS (Hf)) with a chemical formula of [Hf₆O₄(OH)₈L]_{3.5}·xH₂O as the catalyst at 100 °C in dimethyl sulfoxide (DMSO) for 1 h.¹⁴

The production of 2,5-DMF in high yield was demonstrated by using high purity 5-HMF as the starting feed. The seminal work by the Dumesic group in 2007 described the conversion of fructose to 2,5-DMF with a 71 mol% yield using a Cu–Ru/C catalyst in 1-butanol at 0.68 MPa of H₂ and 220 °C for 10 h.¹ Afterwards, Binder *et al.* reported the hydrogenolysis of crude 5-HMF, which was produced from corn stover, to 2,5-DMF with a 49 mol% yield over the same type of catalyst and under similar reaction conditions.² Wang *et al.* determined that Pt–Co nanoparticles on a hollow carbon sphere could provide a 2,5-DMF yield of 98 mol% at 180 °C and 1 MPa of H₂ for 2 h in 1-butanol.¹⁵ The use of formic acid as a source of H₂ as well as an acid catalyst over Pd/C led to the conversion of 5-HMF to

Introduction

Owing to the current global warming issue and rapid depletion of crude oil, renewable biofuels and value-added chemicals derived from biomass are of great interest.^{1–3} Among the various types of bio-derived fuels and chemicals, 2,5-dimethylfuran (2,5-DMF), a derivative of furan, is considered as one of the most promising biofuels because of its clear advantages over the first generation bioethanol, such as a high energy density (30 kJ cm⁻³), research octane number (RON = 119),

^aSKKU Advanced Institute of Nanotechnology (SAINT), Sungkyunkwan University, 2066 Seobu-Ro, Jangan-Gu, Suwon, Gyeong Gi-Do, 16419, Republic of Korea. E-mail: jaehoonkim@skku.edu

^bInstitute of Advanced Composite Materials, Korea Institute of Science and Technology, Chudong-ro 92, Bongdong-eup, Wanju-gun, Jeonranbuk-do, Republic of Korea

^cSchool of Mechanical Engineering, Sungkyunkwan University, 2066 Seobu-Ro, Jangan-Gu, Suwon, Gyeong Gi-Do, 16419, Republic of Korea

†Electronic supplementary information (ESI) available. See DOI: 10.1039/c7gc00269f

2,5-DMF with a high yield of 95 mol%.³ Chidambaram *et al.* found that the low H₂ solubility in a solution of 1-ethyl-3-methylimidazolium chloride ([EMIM]Cl) in acetonitrile over Pd/C resulted in a low 2,5-DMF yield of 0.14 mol% with 32% selectivity at 120 °C and 0.62 MPa of H₂ for 1 h.¹⁶ In order to find a suitable reaction medium for producing high-yield 2,5-DMF, Nagpure *et al.* tested the hydrogenolysis of 5-HMF in various solvents with a different chemical nature, including nonpolar (toluene), polar protic (2-propanol), and polar aprotic (THF, DMSO, and CH₃CN) solvents, over a Ru–Na–Y catalyst, and found that THF was the most promising solvent, producing 70 mol% of 2,5-DMF owing to its reduced interaction with the Ru active sites.¹⁷ Recently, Upare *et al.* reported a 92 mol% overall yield of 2,5-DMF starting from fructose in 1-butanol over Amberlyst-15 (for dehydration of fructose)/Ru–Sn/ZnO (for hydrogenolysis of 5-HMF) catalysts.⁷

Although the high-yield production of 2,5-DMF from fructose has been well-demonstrated using the two-step approach, most of these methods involve a highly energy intensive and costly purification of 5-HMF from the dehydration products prior to its hydrogenolysis,^{18,19} which increases the production cost of 2,5-DMF. Several studies have been dedicated to the one-pot, direct conversion of fructose to 2,5-DMF without the purification of 5-HMF from the dehydration mixture, but the yield of 2,5-DMF was very low.^{2,8–10} For example, the use of CrCl₃ for the dehydration of corn stover, followed by the hydrogenolysis of the crude 5-HMF solution, resulted in only 9 mol% of 2,5-DMF using Cu–Ru/C in butanol at 220 °C for 10 h in a batch reactor.² The one-pot conversion of fructose over ZnCl₂–Pd/C as the catalyst resulted in only 22 mol% of 2,5-DMF in THF at 150 °C and 0.8 MPa H₂ for 8 h.⁸ Xiang *et al.* used a one-flow, two-fixed bed reactor with HY zeolite and Cu/ZnO/Al₂O₃ as dehydration and hydrogenolysis catalysts, respectively, to convert fructose into 2,5-DMF. The resulting 2,5-DMF yield was 40.6 mol% at 240 °C.⁹ Very recently, Wei *et al.* have proposed a direct conversion of fructose to 2,5-DMF with a 66 mol% yield using a combination of homogeneous (AlCl₃/H₂SO₄/H₃PO₄) and heterogeneous (Ru/C) catalysts at 200 °C and 1.5 MPa H₂ for 12 h in *N,N*-dimethylformamide (*N,N*-DMF).²⁰ However, the potential reactor corrosion caused by the strong acid, the treatment of the waste acid, and the difficulty in product separation caused by using a homogeneous-type Brønsted acid should be addressed. In addition, the use of glucose as feed for the direct production of 2,5-DMF in place of fructose has never been reported. A typical method to produce fructose is the enzymatic isomerization of glucose, but the use of huge amounts of enzymes to ensure the high-throughput of fructose and the narrow processing window of isomerization might increase the overall production cost.^{21,22}

Herein, we demonstrate a one-pot, direct conversion of monosaccharides (fructose and glucose) to 2,5-DMF with an unprecedented high yield up to 70.5 mol% over a multifunctional heterogeneous Pd/Zr-based metal–organic framework@-sulfonated graphene oxide catalyst (Pd/Uio-66@SGO) without involving the purification of 5-HMF. In addition, when glucose was used in this one-pot conversion, the 2,5-DMF yield was

still as high as 45.3 mol%. The role of the support and the effect of the reaction parameters (Pd loading, temperature, time) are discussed.

Results and discussion

Catalyst characterization

Fig. S1a† shows the X-ray diffraction (XRD) patterns of the supports and the Pd-loaded catalysts, *e.g.*, sulfonated graphene oxide (SGO), the Zr-based metal–organic framework (UiO-66), UiO-66@SGO, 2.4 wt% Pd loaded on UiO-66@SGO (2.4Pd/UiO@SGO), and 4.8 wt% Pd loaded on UiO-66@SGO (4.8Pd/UiO-66@SGO). The Pd loading was measured using inductively coupled plasma-atomic emission spectroscopy (ICP-OES) (Table S2†). The XRD pattern of the as-synthesized UiO-66 agrees well with that reported in the literature.²³ The XRD patterns of the 2.4Pd/UiO-66@SGO and 4.8Pd/UiO-66@SGO catalysts exhibit three clear peaks at 2θ of 40.1, 46.7, and 68.1°, which correspond to the (111), (200), and (220) planes of the face-centered cubic Pd structure (JCPDS no. 05-0681), respectively. The intensity of the peaks associated with Pd increases with increasing Pd loadings. The crystalline structure of the host UiO-66 was maintained after the incorporation of SGO and impregnation of Pd.

The thermal stabilities of the as-synthesized UiO-66, 2.4Pd/UiO-66@SGO, and 4.8Pd/UiO-66@SGO catalysts were examined by thermogravimetric analysis (TGA) under air flow conditions, as shown in Fig. S1b.† The marginal weight loss (5.6 wt%) of the samples below 100 °C was due to the adsorbed solvent in the framework, while the weight loss at 250–300 °C can be attributed to the reversible dehydration of Zr₆O₄(OH)₄ to Zr₆O₆.^{24,25} The significant weight loss above 450 °C was caused by the decomposition of the organic linker (1,4-benzenedicarboxylic acid) used for the synthesis of UiO-66. The early weight loss of Pd/UiO-66@SGO was probably due to the adsorption of water or volatile species on SGO. A major decomposition of the Pd/UiO-66@SGO catalysts occurred at 425 °C, and it was caused by the decomposition of thermally labile oxygenated species in SGO. Therefore, the TGA profiles of UiO-66 and Pd/UiO-66@SGO indicate the high thermal stability of this support at temperatures below 250 °C.

To investigate the chemical functionality of SGO and the valence state of the Pd atoms in the catalysts, X-ray spectroscopy (XPS) analysis was employed, as shown in Fig. S1c.† The high-resolution C 1s spectrum of SGO indicates at least four types of carbons bonded to different oxygen functional groups: C–O–C (286.8 eV), C–OH (285.8 eV), C=O (287.8 eV), and O=C–O (289.3 eV) along with a highly intense peak of C–C (285.6 eV). The O 1s spectrum was deconvoluted to three peaks at 531.2, 532.6, and 533.7 eV, which were attributed to O=C=O, C–O, and O₂[–], respectively.^{26,27} The deconvoluted S 2p spectrum with two peaks at the binding energies of 168.1 and 169.2 eV, corresponding to the S 2p_{3/2} and S 2p_{1/2} of the sulfonic acid group (SO₃) on SGO,^{27–29} indicates that the sulfonic group has been successfully incorporated on the GO sheets. The Pd 3d spectra of the

Table 1 The textural properties of UiO-66, SGO, and Pd/UiO-66@SGO catalysts^a

Sample	BET surface area (m ² g ⁻¹)	Pore volume (cm ³ g ⁻¹)	Mean pore diameter (nm)
UiO-66 ^b	1318	0.67	2.17
SGO ^b	51	11.8	9.57
UiO-66@SGO ^b	765	0.41	2.20
2.4Pd/UiO-66@SGO ^b	750	0.44	2.65
4.8Pd/UiO-66@SGO ^b	715	0.40	2.74
4.8PdUiO-66@SGO ^c	635	0.25	2.82

^a BET surface area, pore volume, and pore diameter determined by N₂ adsorption at 77 K. ^b Fresh synthesized catalyst. ^c Fifth cycle reused catalyst.

2.4Pd/UiO-66@SGO and 4.8Pd/UiO-66@SGO catalysts clearly show the characteristic peaks of Pd 3d_{3/2} and Pd 3d_{5/2} at 341.0 and 335.6 eV, respectively, which demonstrate the presence of metallic Pd in the catalysts.

Fig. S1d† and Table 1 represent the N₂ adsorption–desorption isotherms of the support and the catalysts. UiO-66 exhibited a type I isotherm with a high surface area of 1318 m² g⁻¹, which is similar to the previously reported values.²³ The pore volume of UiO-66 was 0.67 cm³ g⁻¹. The pore size distribution of UiO-66 was very narrow (0.6–1.2 nm), as shown in Fig. S1e,† indicating a rich microporous structure. The surface area of UiO-66@SGO decreased to 765 m² g⁻¹ because of the contribution of the low surface area of SGO to the support. After the Pd loading, the surface area of the catalysts decreased slightly to 715–750 m² g⁻¹, but the pore size distribution did not change much as compared to their support. This suggests that the Pd deposition extensively occurred on the exterior surface of UiO-66 and the textural properties of the support did not change significantly during the Pd deposition. The Raman spectra of GO and SGO (Fig. S1f†) show the characteristic D and G bands at 1350 and 1597 cm⁻¹, respectively, which correspond to the structural defects and in plane vibration of the sp² carbons, respectively.³⁰ The slight increase in the D-band to G-band ratio (*I_D/I_G*) of SGO (1.06) as compared to GO (0.85) indicates the decreasing of the sp² carbon domain during the sulfonation of GO.

The acid strengths of the catalysts were also analyzed through NH₃ temperature-programmed desorption (TPD); the TPD profiles are shown in Fig. S2† and the corresponding amount of acid sites are listed in Table S2.† The SGO support had a total of 2.28 mmol g⁻¹ acid sites, of which 0.35 mmol g⁻¹ was attributed to weak-medium acid sites (150–300 °C) and 1.93 mmol g⁻¹ to strong acid sites (300–600 °C). The acid sites of Pd/UiO-66@SGO were shifted to strong acid regions (Fig. S2†), suggesting an increase in the Brønsted acidity of the catalyst. The total acidities of 2.4Pd/UiO-66@SGO and 4.8Pd/UiO-66@SGO were 3.16 and 3.21 mmol g⁻¹, respectively. The strong acid sites contributed to over 90% of the total acid sites. As listed in Table S1,† a similar trend can be observed in the titration results.

The morphology of the Pd/UiO-66@SGO catalysts was examined by scanning electron microscopy (SEM) and high-resolu-

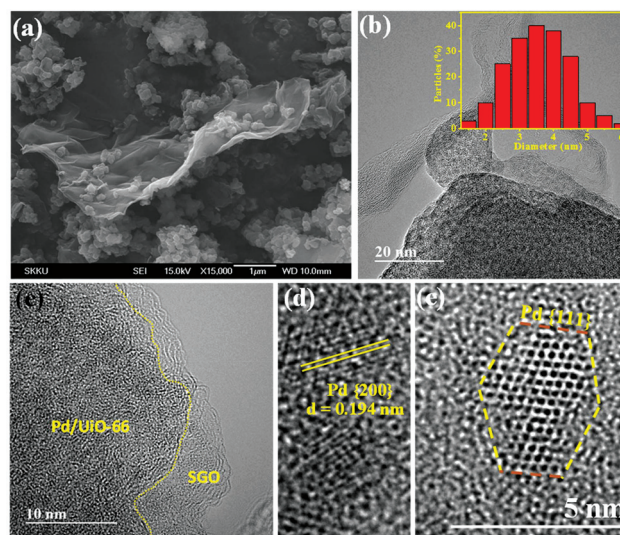


Fig. 1 4.8Pd/UiO-66@SGO catalyst surface morphology: (a) SEM image and (b–e) the corresponding HR-TEM images. The inset in (b) shows the size distribution of Pd.

tion transmission electron microscopy (HR-TEM). The parent UiO-66 was comprised of octahedron particles¹⁴ with a mean size of 200 nm (Fig. S3†). As shown in Fig. 1a, the UiO-66 particles were randomly dispersed on the few layered SGO sheets in the 4.8Pd/UiO-66@SGO catalyst. The HR-TEM image of 4.8Pd/UiO-66@SGO illustrates a uniform distribution of the Pd nanoparticles on the surface of UiO-66 with a mean size of 3.5 ± 0.5 nm. As shown in Fig. S4,† a high population of Pd nanoparticles with sizes of 2–6 nm was deposited on the UiO-66@SGO support when the Pd loading increased to 4.8 wt%. The elemental mapping of 4.8Pd/UiO-66@SGO indicates a uniform distribution of Pd on the UiO-66@SGO surface (Fig. S5†).

Fructose and glucose conversion to 2,5-DMF

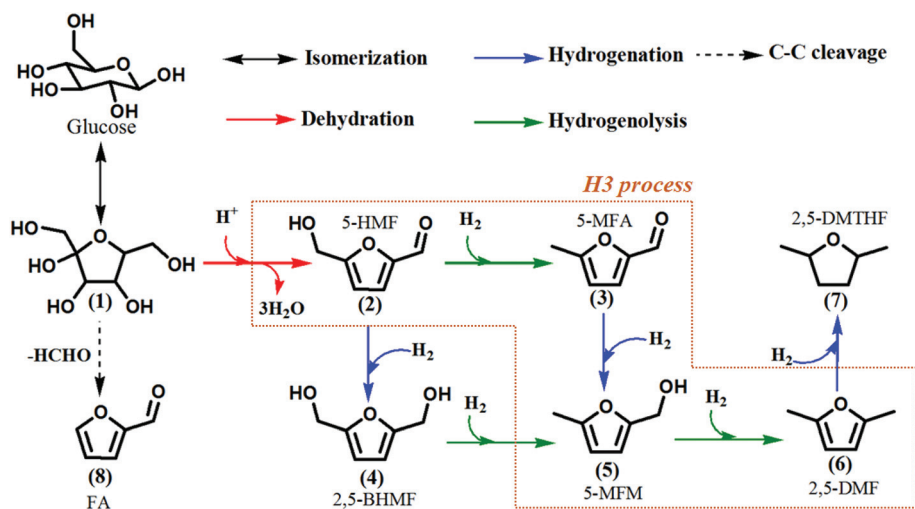
By using the 4.8Pd/UiO-66@SGO catalyst, monosaccharides can directly be converted into high-yield 2,5-DMF. As listed in Table 2, extraordinary high yields of 2,5-DMF were obtained from fructose and glucose (70.5 and 45.3 mol%, respectively) at temperatures of 160–180 °C and 1 MPa H₂ in THF for 3 h. The use of 5-HMF as feedstock resulted in an almost complete 2,5-DMF yield of 99.2% at 160 °C for 3 h.

The reaction mixtures were analyzed using gas chromatography-time-of-flight mass spectroscopy (GC-TOF/MS) to understand the reaction pathway from fructose to 2,5-DMF over the Pd/UiO-66@SGO catalyst. The reaction intermediates (5-hydroxymethylfurfural, 5-HMF; 5-methylfurfural, 5-MFA; 5-methyl-furanmethanol, 5-MFM), the by-product (furfural, FA), the final product (2,5-DMF), and the over-hydrogenated product (2,5-dimethyltetrahydrofuran, 2,5-DMTHF) were identified in the reaction mixtures. Plausible reaction pathways for the direct conversion of glucose and fructose over Pd/UiO-66@SGO are shown in Scheme 1.

Table 2 Monosaccharide conversion to 2,5-dimethylfuran^a

Entry	Reactant	Catalyst	Reaction conditions			Conversion (%)	Yield (mol%)					Selectivity ^f (%)
			T (°C)	Time (h)	P (MPa)		5-HMF	FA	5-MFA	2,5-DMF	2,5-DMTHF	
1	Fructose	No catalyst	200	3	1	33.3	—	Trace	—	—	n.d. ^e	—
2		GO	200	3	1	80.8	8.6	35.3	n.d.	n.d.	n.d.	—
3		SGO	200	3	1	83.0	23.6	29.4	n.d.	n.d.	n.d.	—
4a		UiO-66	200	3	1	87.4	35.2	32.1	n.d.	n.d.	n.d.	—
4b		UiO-66 ^b	200	3	1	55.3	10.7	38.3	n.d.	n.d.	n.d.	—
5		UiO-66/SGO	200	3	1	90.5	55.9	19.3	n.d.	n.d.	n.d.	—
6		4.8Pd/SGO	160	3	1	88.1	Trace	Trace	9.6	38.5	24.0	43.6
7		2.4Pd/UiO-66@SGO	160	1	1	77.5	18.5	Trace	36.1	25.9	n.d.	33.4
8			160	3	1	85.2	Trace	Trace	8.6	68.6	n.d.	83.8
9			160	5	1	89.6	Trace	Trace	9.7	55.3	n.d.	62.0
10			160	3	0.3	78.6	21.4	Trace	16.7	46.4	n.d.	59.3
11		4.8Pd/UiO-66@SGO	160	3	1	91.8	Trace	Trace	7.8	70.5	Trace	76.8
12 ^c	Glucose	4.8Pd/UiO-66@SGO	180	3	1	87.3	5.10	Trace	18.0	45.3	Trace	63.8
13 ^d	5-HMF	4.8Pd/UiO-66@SGO	160	3	1	99.9	n.d.	n.d.	Trace	99.2	n.d.	99.3
14	5-HMF	4.8Pd/SGO	160	3	1	99.2	n.d.	n.d.	Trace	68.0	31.0	67.5

^a Standard reaction conditions: 0.2 g (1.1 mmol) feed, 0.2 g catalyst, and 40 mL THF. ^b Synthesized using the method in the ref. 34. ^c 0.18 g (1 mmol) glucose. ^d 0.12 g (1 mmol) 5-HMF. ^e Not detectable. ^f 2,5-DMF selectivity = mol of 2,5-DMF/(mol of reactant – mol of unreacted reactant) × 100.



Scheme 1 Plausible reaction mechanism pathways for glucose conversion to 2,5-dimethylfuran. (1) Fructose; (2) 5-hydroxymethylfural (5-HMF); (3) 5-methylfural (5-MFA); (4) 2,5-bis(hydroxymethyl)-furan (2,5-BHMF); (5) 5-methyl-furanmethanol (5-MFM); (6) 2,5-dimethylfuran (2,5-DMF); (7) 2,5-dimethyltetrahydrofuran (2,5-DMTHF); (8) furfural (FA). The H3 process indicates hydrogenolysis/hydrogenation/hydrogenolysis.

To investigate the roles of the Pd/UiO-66@SGO catalyst and the reaction medium in the direct conversion of fructose, several control experiments were conducted. First, in order to find a preferable fructose dehydration medium, blank experiments (in the absence of a catalyst) were conducted in polar protic (methanol, ethanol, and isopropyl alcohol) and aprotic (tetrahydrofuran) solvents, and the production of furanic compounds was monitored, as shown in Fig. S6.† Based on the area% of the detected compound in the GC-TOF/MS chromatogram, the conversion of fructose at 200 °C and 1 MPa H₂ in THF after 3 h resulted in a much higher area% of furanic compounds (e.g., furfural, 13.3%) as compared to those obtained in alcoholic media under identical conditions (only traces). This is in good agreement with previous reports according to

which the use of polar aprotic solvents (THF,³ DMSO,¹⁴ and *N,N*-DMF²⁰) resulted in high-yield 2,5-DMF from 5-HMF by avoiding the ring-opening of 5-HMF to levulinic acid derivatives.

In the absence of a catalyst, the conversion of fructose in THF was 33.3 mol%, but 5-HMF was not observed (entry 1, Table 2 and Fig. S6d†). Instead, hydroxypropanone, furfural, butyrolactone, 1,6-anhydrofructofuranoside, and butylated hydroxytoluene were produced. In the presence of GO, the fructose conversion increased to 80.8 mol%, but only a small amount of 5-HMF was produced (8.6 mol%, entry 2, see Fig. S7a† for the chromatogram). On the other hand, a high amount of furfural was detected, which can be formed by the cleavage of the C–C bonds of acyclic hexoses followed by the

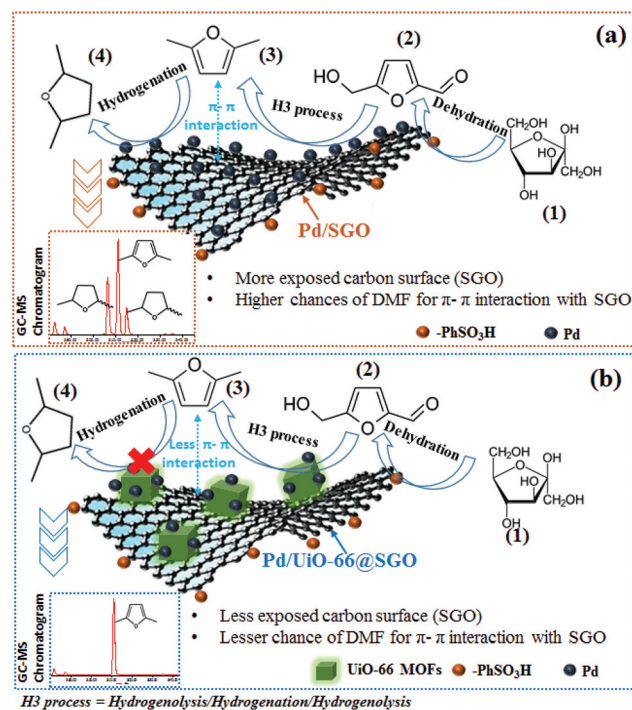
dehydration of pentoses.^{31,32} The use of SGO increased the 5-HMF yield to 23.6 mol%, indicating the activation of the 5-HMF pathway by the presence of the Brønsted acid sites associated with the sulfonated functional group on GO;³³ the total acid density of SGO, originated from $-\text{COOH}$, $-\text{OH}$, and $-\text{SO}_3\text{H}$ groups, was estimated to be 1.95 mmol g^{-1} , while the acidity deriving from the $-\text{SO}_3\text{H}$ group was 1.17 mmol g^{-1} ; these values are higher than those of the bare GO (Table S2†). The fructose conversion using UiO-66 (entry 4a) in the absence of an external Brønsted acid source resulted in a high fructose conversion of 87.4% with a high HMF yield of 35.2 mol%. It is noted that these values are much higher than the fructose conversion over the UiO-66 synthesized without using HCl³⁴ (entry 4b). This exceptional phenomenon can be explained by the nature of the crystal structure of UiO-66. In this work, UiO-66 was synthesized according to Katz *et al.*²³ with additional HCl, and it was proved to exhibit the natural defects of UiO-66 (Fig. S9†). The defected UiO-66 exhibited higher total acidity (1.85 mmol g^{-1}) than that of the ideally closed-packed UiO-66³⁴ (1.31 mmol g^{-1}), as listed in Table S2.† Due to the missing linkers (1,4-benzenedicarboxylic acid) in the UiO-66 framework, this imperfection leads to a large surface area of $1318 \text{ m}^2 \text{ g}^{-1}$ as compared to the ideally closed-packed UiO-66 ($1187 \text{ m}^2 \text{ g}^{-1}$).³⁴ The large surface area of the defected UiO-66 with a high degree of open framework (which is caused by uncoordinated Zr_6 -cluster nodes³⁵) can provide a synergetic effect of Lewis (the Zr^{4+} metal center) and Brønsted (hydroxyl ($\text{Zr}-\text{OH}$)) acids or aquo ($\text{Zr}-\text{OH}_2$ terminal groups) sites in a single material.³⁶

As listed in entry 5 of Table 2 and shown in Fig. S7d,† the UiO-66@SGO support (with a 1 : 1 weight ratio) was also able to produce a high conversion of fructose (90.5%) into the medium yield of 5-HMF (55.9 mol%), since the combinatorial benefits of SGO (Brønsted acid, hydrophilic surface) and UiO-66 (high porosity, high surface area, high acidity) can enhance the fructose adsorption onto the surface of the catalyst (Fig. S10†). Yet, in the absence of a noble metal phase, the further hydrogenation of 5-HMF to 5-MFA was not observed.

The use of 4.8Pd/UiO-66@SGO provided a considerably high yield of 2,5-DMF from fructose (70.5 mol%, entry 11, Fig. S8c†). The presence of 5-MFA in the reaction mixture and the trace amount of 5-MFM detected in the chromatogram (less than 0.1 area%) may imply that the 5-MFA pathway is dominant over 4.8Pd/UiO-66@SGO. In contrast, the use of 4.8Pd/SGO (without UiO-66) resulted in a lower fructose conversion (88.1%) and 2,5-DMF yield (38.5 mol%, entry 6, Fig. S8b†) as compared to those resulting from the use of 4.8Pd/UiO66@SGO. The low 2,5-DMF selectivity over 4.8Pd/SGO was due to the extensive hydrogenation of 2,5-DMF over the Pd surface, leading to the saturation of the double bond in 2,5-DMF to produce 2,5-DMTHF with a relatively high yield (24 mol%). This phenomenon is possibly caused by the high 2,5-DMF adsorption uptake over SGO. To investigate the adsorption selectivity of 2,5-DMF over 2,5-DMTHF on 4.8Pd/SGO and 4.8Pd/UiO-66@SGO, the adsorption selectivity coefficients of 2,5-DMF to 2,5-DMTHF were calculated when

the adsorption of both the components reached an equilibrium point³⁷ (which was achieved after 60 min of adsorption), as shown in Fig. S11.† The Pd/SGO catalyst has an almost two times higher adsorption selectivity coefficient of 2,5-DMF over 2,5-DMTHF (2.32) than that of the Pd/UiO-66@SGO catalyst (1.22), indicating that 2,5-DMF adsorbs more preferentially on Pd/SGO with respect to 2,5-DMTHF as compared to Pd/UiO66@SGO.

As illustrated in Scheme 2, the high 2,5-DMF adsorption uptake on the SGO surface can be caused by the π - π interaction between the furan unsaturated ring and the $\text{C}=\text{C}$ sp^2 of the graphitic carbon. A previous report indicates that the $\text{C}=\text{C}$ sp^2 in the GO structure can allow a strong π - π interaction with aromatic compounds, and in the presence of Pd nanoparticles, the unsaturated $\text{C}=\text{C}$ bond of the aromatic substrate can be readily hydrogenated to its corresponding saturated form.³⁷ On the other hand, in the case of 4.8Pd/UiO-66@SGO, the π - π interaction could be suppressed by the presence of high surface area microporous UiO-66, which could inhibit the excessive hydrogenation favoring a high 2,5-DMF selectivity. In order to evaluate our hypothesis, the 5-HMF conversion was performed using the same reaction conditions (entry 13, Fig. S8d†); an excellent catalyst performance with >99.9% of 5-HMF conversion and 99.2 mol% of 2,5-DMF yield was observed. In contrast, the use of 4.8Pd/SGO resulted in a substantial amount of 2,5-DMTHF (31.0 mol%, entry 14). This result confirms that the ring saturation of 2,5-DMF to



Scheme 2 Schematic illustration of the 2,5-DMF interaction on the catalyst surface, the conversion route through a hydrogenolysis–hydrogenation–hydrogenolysis (H3) process, and the corresponding GC-TOF/MS chromatograms. (a) Pd@SGO catalyst and (b) Pd/UiO-66@SGO.

2,5-DMTHF was suppressed over 4.8Pd/UiO66@SGO even with 5-HMF, whose potential adsorption on the SGO surface might be higher than that of fructose because of its smaller size. Therefore, the high yield production of 2,5-DMF directly from 5-HMF is due to the coordination of the reactant to the well-dispersed metallic Pd sites deposited on the UiO-66 framework (Scheme 2). Recent density functional theory studies^{38,39} suggest the preferable coordination of reactants on the Pd surface. Three types of preferable conformations were suggested; flat (substrate bound *via* its furan ring and the carbonyl group), tilted (substrate bound *via* either its furan ring or the carbonyl group) and vertical (substrate bound *via* oxygen in the furan ring) conformations of furanic compounds on the Pd (111) surface.³⁸ These binding conformations were affected by the presence of a hydrogen co-feed, which assisted the hydrogenolysis reaction. In the ultrahigh vacuum experiment, furanic substrates preferred the flat conformation on the surface of Pd (111),³⁸ while the conformation was tilted on the crowded surface of the hydrogen-covered Pd (111).³⁹ Finally, under moderate pressure and temperature conditions, the furfural conformational changes on the Pd (111) surface were preferred to produce highly selective decarbonylated species.³⁹

As listed in entries 7–9, as the reaction time increased from 1 to 3 h over the 2.4Pd/UiO-66@SGO catalyst, the 2,5-DMF yield also increased from 25.9 to 68.6 mol%; however further increases in the reaction time led to a decrease in the 2,5-DMF yield to 55.3 mol% owing to side reactions. Nonetheless, even after 5 h, the formation of 2,5-DMTHF was not observed, indicating the suppression of excess hydrogenation. When the H₂ pressure was reduced from 1 to 0.3 MPa, the fructose conversion and the 2,5-DMF yield decreased to 78.6% and 46.4 mol%, respectively.

Since a large quantity of the enzyme (*e.g.*, D-glucose/xylose isomerase) and careful control of the process parameters (*e.g.*, temperature, pH) are required to meet the high-throughput production of fructose from glucose by reversible isomerization,^{21,22} the direct conversion of glucose to 2,5-DMF would be more beneficial. As compared to the fructose conversion (entries 11 and 12), the use of glucose resulted in a lower conversion (87.3%) and 2,5-DMF yield (45.3 mol%), while affording a higher 5-MFA yield (18.0 mol%). Apparently, the additional isomerization step would require longer reaction times to achieve a high 2,5-DMF yield.

The conversion of glucose and fructose and yields of main reaction intermediates and products with varying reaction times from 10 to 300 min are shown in Fig. 2. The main chemical species were fructose (when glucose was used), 5-HMF, and 5-MFA. Only a trace amount of 5-MFM was detected in the chromatograms, and thus the 5-MFM yield is not shown in the figure. With increasing reaction time, the 5-HMF yield decreased, while the yields of 5-MFA and 2,5-DMF increased. This confirms the reaction mechanism proposed in Scheme 1. In Fig. 2, the other compounds include tetrahydrofurans, ketones and alcohols, as listed in Table S4 in the ESI.† The activation energies (Fig. S12a and b†) reveal that fructose

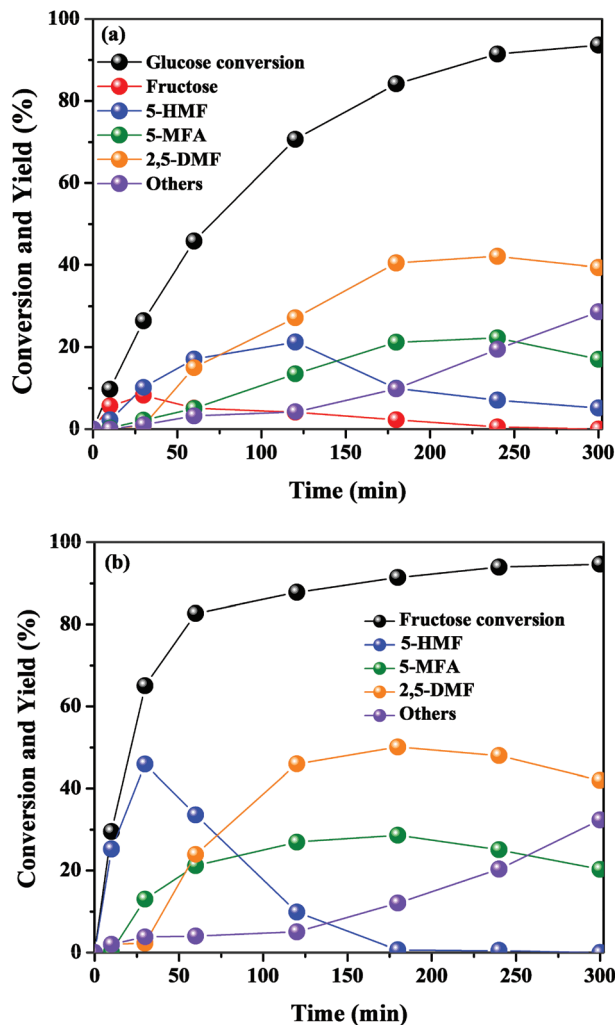


Fig. 2 The conversion of (a) glucose and (b) fructose and yields of the main reaction intermediates and products with varying reaction times. Reaction conditions: 0.2 g feed, 0.2 g 2.4Pd/UiO-66@SGO, 40 mL THF, 180 °C, 1 MPa H₂. 5-HMF, 5-hydroxymethylfurfural; 5-MFA, 5-methylfurfural; and 2,5-DMF, 2,5-dimethylfuran.

can be more readily converted into 5-HMF (80.47 kJ mol⁻¹) as compared to glucose (100.99 kJ mol⁻¹). At low glucose and fructose conversion at a short reaction time of 10 min, the major products were 5-HMF and unconverted monosaccharides, as listed in Table S5.†

To find out the possible side reactions in fructose conversion at extended reaction times, the conversion reaction was prolonged for 7 h; the final product contained a noticeable amount of ketones (*e.g.*, 1-hydroxy-2-propanone, 2,5-hexanedione, 2-methylcyclopentanedione). These components could be produced by the C–C cleavage of C6 to C3, ring-opening of 2,5-DMF, and/or intramolecular aldol reaction of 2,5-hexanedione.⁴⁰

According to the GC-TOF/MS results, the possible pathways of glucose and fructose conversion to produce 2,5-DMF over the Pd/UiO66@SGO catalyst are presented in Scheme 1. In the presence of Lewis acid sites (*e.g.*, CrCl₃), glucose can be firstly

isomerized to fructose and subsequently dehydrated over a Brønsted acid medium (e.g., aqueous HCl) to 5-HMF.¹¹ In this work, the dehydration step is efficiently activated by SGO, which contains a high density of hydrophilic groups such as -COOH and -OH as well as the Brønsted acidic sites of -SO₃H.⁴¹ The fructose molecule can be readily adsorbed onto the SGO surface³⁰ or in between the SGO layers trapped inside the hydrophobic cage and then dehydrated to form 5-HMF.⁴² Two plausible reaction pathways from 5-HMF to 2,5-DMF involving two different types of intermediates have been reported and well-summarized in previous work;²⁰ either 2,5-bis(hydroxymethyl)furan (2,5-BHMF) can be formed by hydrogenation of the aldehyde group in 5-HMF, or 5-MFA can be produced by the hydrogenolysis of the hydroxyl group in 5-HMF. Subsequently, in the presence of a metal catalyst under a H₂ atmosphere, either 2,5-BHMF can be hydrogenolyzed or 5-MFA can be hydrogenated to form 5-MFM. As shown in Fig. S6,† 2,5-BHMF was not observed in the product mixture, thus the 5-MFA pathway is believed to be the dominant reaction over the Pd/UiO-66@SGO catalyst. A further hydrogenolysis reaction can occur to cleave the hydroxyl group in 5-MFM to form 2,5-DMF.

The effect of the reaction temperature on the conversion and product yields over the 2.4Pd/UiO-66@SGO catalyst is shown in Fig. 3. The fructose and glucose conversions increased up to 90% upon a temperature increase from 140 to 200 °C. When using fructose as the reactant, the 2,5-DMF yield increased significantly from 35.4 to 68.6 mol% with increases in temperature from 140 to 160 °C, while further increases of temperature to 180 and 200 °C resulted in the reduction of the 2,5-DMF yield to 47.1 and 30.4 mol%, respectively. As shown

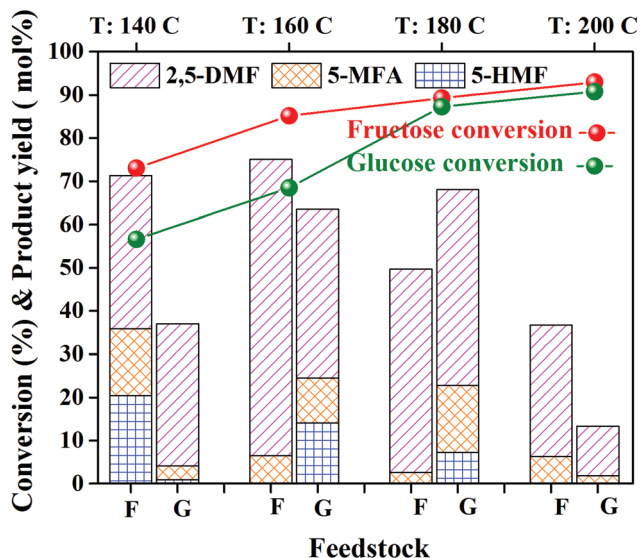


Fig. 3 Effect of reaction temperature on fructose and glucose conversions and product yields. Reaction conditions: 0.2 g feed; 0.2 g 2.4Pd/UiO-66@SGO; 40 mL THF, at 160 °C 3 h, 1 MPa H₂. 5-HMF, 5-hydroxymethylfurfural; 5-MFA, 5-methylfurfural; and 2,5-DMF, 2,5-dimethylfuran.

in Fig. S13a and b,† 2-methyltetrahydrofuran, 1-hydroxy-propanone, and 2,5-hexanedione were detected by GC-TOF/MS, and could be produced by side reactions including excess hydrogenation, C-C cleavage, and furan ring-opening at a high reaction temperature regime. When glucose was used over the 2.4Pd/UiO-66@SGO catalyst, a maximum 2,5-DMF yield of 43.2 mol% was achieved at 180 °C, and a further increase of the temperature to 200 °C resulted in a significant drop of the 2,5-DMF yield to 11.5 mol%. Again, the side products detected in the GC-TOF/MS chromatograms (Fig. S13c,† 3-hydroxy-2-butanone, hydroxy-propanone, 3-methylcyclopentanone, and 3-methylcyclopent-2-enone) can be caused by side reactions.

To investigate the reusability of the Pd loaded on UiO-66@SGO, the 4.8Pd/UiO-66@SGO catalyst was tested over five cycles of fructose and glucose conversion at 160 °C for 3 h under 1 MPa H₂ in THF. After each cycle, the recovered catalyst was washed several times with THF, acetone, methanol, and finally water to remove the unreacted substrate, dried at 70 °C for 6 h, and then reused in the next cycle. As shown in Fig. 4, the fructose conversion activity could be well maintained for up to five cycles of the reusability test. The 2,5-DMF yield decreased somewhat rapidly from 70.5 to 58.3 mol% in the second run, while decreasing only slightly to 52.1 mol% in the subsequent cycles. On the other hand, the 5-HMF yield increased somewhat rapidly from 5.6 to 14.2 mol% in the second run, and slowly to 19.8 mol% up to the fifth run. This suggests that as the number of cycles increased, the fructose dehydration activity was maintained, but some of the formed 5-HMF was not converted to 2,5-DMF. In the case of glucose conversion, the 2,5-DMF yield slowly decreased from 45.3 to 35.0 mol%, while the 5-HMF yield slightly increased from 6.5 to 7.5 mol% during five-cycle reactions. After the fifth run, the catalyst was recovered and analyzed; as shown in Fig. S14a,†

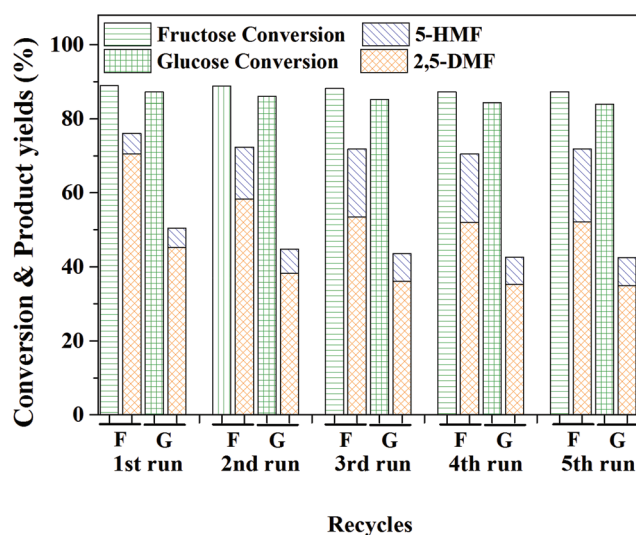


Fig. 4 Catalyst recyclability test. Reaction conditions: 0.2 g feed, 0.2 g 4.8Pd/UiO-66@SGO; 40 mL THF, 160 °C (fructose) and 180 °C (glucose), 3 h, 1 MPa H₂. 5-HMF, 5-hydroxymethylfurfural; 2,5-DMF, 2,5-dimethylfuran.

the high crystallinity of the spent catalyst indicates that the UiO-66 framework remained almost unchanged during the reaction, which can be the reason for the high fructose conversion and 2,5-DMF yield. The oxygen and sulfur contents in the spent catalyst, measured using elemental analysis, were very similar to those of the fresh catalyst (Table S6†), suggesting a good stability of the acid sites in SGO. As shown in Fig. S14b, c† and Table 1, the BET surface of the spent catalyst decreased slightly from 715 to 635 m² g⁻¹, while the pore volume decreased from 0.40 to 0.25 cm³ g⁻¹, indicating that the reaction lowered the exposed surface area. In addition, the Pd content in the spent catalyst decreased to 4.3 wt%, indicating that some degree of Pd leaching occurred during the reaction. This indicates that the loss of catalytic activity after the 2nd run can be caused by Pd leaching because of the lack of proper binding sites on the surface of the UiO-66 framework. To suppress the Pd nanoparticle leaching, it would be necessary to modify the structure of the UiO-66 framework using electron-donating functionalized terephthalate linkers.^{43,44} The decrease in the surface area and the Pd leaching can also be responsible for the slight reduction of the hydrogenolysis/hydrogenation.

Conclusion

In summary, we have developed a one-pot strategy for producing high-yield 2,5-DMF directly from monosaccharides (fructose and glucose) over a highly efficient Pd loaded integrated Zr-metal organic framework@sulfonated graphene oxide catalyst. Along with SGO, the defected UiO-66 could provide additional Brønsted acid sites, which resulted in high-yield 5-HMF by the dehydration of fructose. The produced 5-HMF in the reaction mixture was further converted to 2,5-DMF over Pd nanoparticles by the hydrogenation/hydrogenolysis of 5-HMF. From the fructose feed, a maximum 2,5-DMF yield of 70.5 mol% was achieved at 160 °C in tetrahydrofuran in 3 h without purification of the intermediate 5-HMF. When glucose was used, the 2,5-DMF yield was 45.3 mol% under identical reaction conditions because of the additional isomerization step. A reusability test of the Pd/UiO-66@SGO catalyst indicated that the 2,5-DMF yield over the first two runs decreased slightly to 58.3 mol%, but remained at 52.1 mol% over the last three runs. It was suggested that the direct conversion of fructose to 2,5-DMF over Pd/UiO-66@SGO is highly efficient and simple, and could promote the use of 2,5-DMF as a renewable alternative to gasoline in the transportation sector and as a building block for value-added chemicals.

Acknowledgements

This study was supported by a National Research Foundation of Korea (NRF) grant funded by the Korean Government (MSIP) (no. 2016R1A2B3008800, 2015H1D3A1066544, and 2016R1D1A1B03934060). Additional support by the New &

Renewable Energy Core Technology Program (no. 20143030090940) of the Korea Institute of Energy Technology Evaluation and Planning (KETEP) financed by the Ministry of Trade, Industry, and Energy, Republic of Korea is appreciated.

References

- 1 Y. Román-Leshkov, C. J. Barrett, Z. Y. Liu and J. A. Dumesic, *Nature*, 2007, **447**, 982–985.
- 2 J. B. Binder and R. T. Raines, *J. Am. Chem. Soc.*, 2009, **131**, 1979–1985.
- 3 T. Thananathanachon and T. B. Rauchfuss, *Angew. Chem., Int. Ed.*, 2010, **49**, 6616–6618.
- 4 S. Zhong, R. Daniel, H. Xu, J. Zhang, D. Turner, M. L. Wyszynski and P. Richards, *Energy Fuels*, 2010, **24**, 2891–2899.
- 5 I. F. Teixeira, B. T. W. Lo, P. Kostetsky, M. Stamatakis, L. Ye, C. C. Tang, G. Mpourmpakis and S. C. E. Tsang, *Angew. Chem., Int. Ed.*, 2016, **55**, 13061–13066.
- 6 C. L. Williams, C.-C. Chang, P. Do, N. Nikbin, S. Caratzoulas, D. G. Vlachos, R. F. Lobo, W. Fan and P. J. Dauenhauer, *ACS Catal.*, 2012, **2**, 935–939.
- 7 P. P. Upare, D. W. Hwang, Y. K. Hwang, U. H. Lee, D.-Y. Hong and J.-S. Chang, *Green Chem.*, 2015, **17**, 3310–3313.
- 8 B. Saha, C. M. Bohn and M. M. Abu-Omar, *ChemSusChem*, 2014, **7**, 3095–3101.
- 9 X. Xiang, J. Cui, G. Ding, H. Zheng, Y. Zhu and Y. Li, *ACS Sustainable Chem. Eng.*, 2016, **4**, 4506–4510.
- 10 G.-Y. Jeong, A. K. Singh, S. Sharma, K. W. Gyak, R. A. Maurya and D.-P. Kim, *NPG Asia Mater.*, 2015, **7**, e173.
- 11 V. Choudhary, S. H. Mushrif, C. Ho, A. Anderko, V. Nikolakis, N. S. Marinkovic, A. I. Frenkel, S. I. Sandler and D. G. Vlachos, *J. Am. Chem. Soc.*, 2013, **135**, 3997–4006.
- 12 L. Hu, X. Tang, J. Xu, Z. Wu, L. Lin and S. Liu, *Ind. Eng. Chem. Res.*, 2014, **53**, 3056–3064.
- 13 J. M. R. Gallo, D. M. Alonso, M. A. Mellmer and J. A. Dumesic, *Green Chem.*, 2013, **15**, 85–90.
- 14 Z. Hu, Y. Peng, Y. Gao, Y. Qian, S. Ying, D. Yuan, S. Horike, N. Ogiwara, R. Babarao and Y. Wang, *Chem. Mater.*, 2016, **28**, 2659–2667.
- 15 G.-H. Wang, J. Hilgert, F. H. Richter, F. Wang, H.-J. Bongard, B. Spliethoff, C. Weidenthaler and F. Schüth, *Nat. Mater.*, 2014, **13**, 293–300.
- 16 M. Chidambaram and A. T. Bell, *Green Chem.*, 2010, **12**, 1253–1262.
- 17 A. S. Nagpure, N. Lucas and S. V. Chilukuri, *ACS Sustainable Chem. Eng.*, 2015, **3**, 2909–2916.
- 18 Y. Román-Leshkov, J. N. Chheda and J. A. Dumesic, *Science*, 2006, **312**, 1933–1937.
- 19 J. Wang, J. Ren, X. Liu, G. Lu and Y. Wang, *AIChE J.*, 2013, **59**, 2558–2566.
- 20 Z. Wei, J. Lou, Z. Li and Y. Liu, *Catal. Sci. Technol.*, 2016, **6**, 6217–6225.
- 21 Y. Wang, Y. Pan, Z. Zhang, R. Sun, X. Fang and D. Yu, *Process Biochem.*, 2012, **47**, 976–982.

- 22 S. H. Bhosale, M. B. Rao and V. V. Deshpande, *Microbiol. Rev.*, 1996, **60**, 280–300.
- 23 M. J. Katz, Z. J. Brown, Y. J. Colón, P. W. Siu, K. A. Scheidt, R. Q. Snurr, J. T. Hupp and O. K. Farha, *Chem. Commun.*, 2013, **49**, 9449–9451.
- 24 L. Valenzano, B. Civalleri, S. Chavan, S. Bordiga, M. H. Nilsen, S. Jakobsen, K. P. Lillerud and C. Lamberti, *Chem. Mater.*, 2011, **23**, 1700–1718.
- 25 H. Wu, Y. S. Chua, V. Krungleviciute, M. Tyagi, P. Chen, T. Yildirim and W. Zhou, *J. Am. Chem. Soc.*, 2013, **135**, 10525–10532.
- 26 S. Biniak, G. Szymański, J. Siedlewski and A. Świątkowski, *Carbon*, 1997, **35**, 1799–1810.
- 27 C. Petit, M. Seredych and T. J. Bandosz, *J. Mater. Chem.*, 2009, **19**, 9176–9185.
- 28 A. J. Crisci, M. H. Tucker, M.-Y. Lee, S. G. Jang, J. A. Dumesic and S. L. Scott, *ACS Catal.*, 2011, **1**, 719–728.
- 29 P. P. Upare, J.-W. Yoon, M. Y. Kim, H.-Y. Kang, D. W. Hwang, Y. K. Hwang, H. H. Kung and J.-S. Chang, *Green Chem.*, 2013, **15**, 2935–2943.
- 30 D. Verma, R. Tiwari and A. K. Sinha, *RSC Adv.*, 2013, **3**, 13265–13272.
- 31 J. Cui, J. Tan, T. Deng, X. Cui, Y. Zhu and Y. Li, *Green Chem.*, 2016, **18**, 1619–1624.
- 32 F. Jin and H. Enomoto, *Energy Environ. Sci.*, 2011, **4**, 382–397.
- 33 Q. Hou, W. Li, M. Ju, L. Liu, Y. Chen and Q. Yang, *RSC Adv.*, 2016, **6**, 104016–104024.
- 34 J. H. Cavka, S. Jakobsen, U. Olsbye, N. Guillou, C. Lamberti, S. Bordiga and K. P. Lillerud, *J. Am. Chem. Soc.*, 2008, **130**, 13850–13851.
- 35 F. Vermoortele, B. Bueken, G. L. Le Bars, B. Van de Voorde, M. Vandichel, K. Houthoofd, A. Vimont, M. Daturi, M. Waroquier and V. Van Speybroeck, *J. Am. Chem. Soc.*, 2013, **135**, 11465–11468.
- 36 M. Rimoldi, A. J. Howarth, M. R. DeStefano, L. Lin, S. Goswami, P. Li, J. T. Hupp and O. K. Farha, *ACS Catal.*, 2016, **7**, 997–1014.
- 37 Z. Wei, R. Pan, Y. Hou, Y. Yang and Y. Liu, *Sci. Rep.*, 2015, **5**, 15664.
- 38 V. Vorotnikov, G. Mpourmpakis and D. G. Vlachos, *ACS Catal.*, 2012, **2**, 2496–2504.
- 39 S. Wang, V. Vorotnikov and D. G. Vlachos, *ACS Catal.*, 2014, **5**, 104–112.
- 40 E. R. Sacia, M. H. Deaner and A. T. Bell, *Green Chem.*, 2015, **17**, 2393–2397.
- 41 S. Suganuma, K. Nakajima, M. Kitano, D. Yamaguchi, H. Kato and S. Hayashi, *J. Am. Chem. Soc.*, 2008, **130**, 12787–12793.
- 42 Z. Wei, Y. Yang, Y. Hou, Y. Liu, X. He and S. Deng, *ChemCatChem*, 2014, **6**, 2354–2363.
- 43 V. Pascanu, Q. Yao, A. Bermejo Gómez, M. Gustafsson, Y. Yun, W. Wan, L. Samain, X. Zou and B. Martín-Matute, *Chem. – Eur. J.*, 2013, **19**, 17483–17493.
- 44 L. Chen, H. Chen, R. Luque and Y. Li, *Chem. Sci.*, 2014, **5**, 3708–3714.